01 Dec 2015

Hierarchical Segmentation of the Malawi Rift: The Influence of Inherited Lithospheric Heterogeneity and Kinematics in the Evolution of Continental Rifts

Daniel A. Lao-Davila

Haifa S. Al-Salmi

Mohamed G. Abdel Salam
Missouri University of Science and Technology, abdelsam@mst.edu

Estella A. Atekwana
Missouri University of Science and Technology, atekwana@mst.edu

Recommended Citation

D. A. Lao-Davila et al., "Hierarchical Segmentation of the Malawi Rift: The Influence of Inherited Lithospheric Heterogeneity and Kinematics in the Evolution of Continental Rifts," *Tectonics*, vol. 34, no. 12, pp. 2399-2417, American Geophysical Union (AGU), Dec 2015.
The definitive version is available at https://doi.org/10.1002/2015TC003953

AGU PUBLICATIONS

Tectonics

RESEARCH ARTICLE
10.1002/2015TC003953

Key Points:
- Segmentation of the Malawi Rift is studied using SRTM DEM and magnetic data
- The rift is hierarchically divided into first-order and second-order segments
- Lithospheric heterogeneity controls first- and second-order segmentation

Correspondence to:
D. A. Laó-Dávila,
daniel.lao_davila@okstate.edu

Citation:
Laó-Dávila, D. A., H. S. Al-Salmi, M. G. Abdelsalam, and E. A. Atekwana (2015), Hierarchical segmentation of the Malawi Rift: The influence of inherited lithospheric heterogeneity and kinematics in the evolution of continental rifts, *Tectonics*, *34*, 2399–2417, doi:10.1002/2015TC003953.

Received 20 JUN 2015
Accepted 16 NOV 2015
Accepted article online 20 NOV 2015
Published online 11 DEC 2015

Hierarchical segmentation of the Malawi Rift: The influence of inherited lithospheric heterogeneity and kinematics in the evolution of continental rifts

Daniel A. Laó-Dávila[1], Haifa S. Al-Salmi[1], Mohamed G. Abdelsalam[1], and Estella A. Atekwana[1]

[1]Boone Pickens School of Geology, Oklahoma State University, Stillwater, Oklahoma, USA

Abstract We used detailed analysis of Shuttle Radar Topography Mission-digital elevation model and observations from aeromagnetic data to examine the influence of inherited lithospheric heterogeneity and kinematics in the segmentation of largely amagmatic continental rifts. We focused on the Cenozoic Malawi Rift, which represents the southern extension of the Western Branch of the East African Rift System. This north trending rift traverses Precambrian and Paleozoic-Mesozoic structures of different orientations. We found that the rift can be hierarchically divided into first-order and second-order segments. In the first-order segmentation, we divided the rift into Northern, Central, and Southern sections. In its Northern Section, the rift follows Paleoproterozoic and Neoproterozoic terrains with structural grain that favored the localization of extension within well-developed border faults. The Central Section occurs within Mesoproterozoic-Neoproterozoic terrain with regional structures oblique to the rift extent. We propose that the lack of inherited lithospheric heterogeneity favoring extension localization resulted in the development of the rift in this section as a shallow graben with undeveloped border faults. In the Southern Section, Mesoproterozoic-Neoproterozoic rocks were reactivated and developed the border faults. In the second-order segmentation, only observed in the Northern Section, we divided the section into five segments that approximate four half-grabens/asymmetrical grabens with alternating polarities. The change of polarity coincides with flip-over full-grabens occurring within overlap zones associated with ~150 km long alternating border faults segments. The inherited lithospheric heterogeneity played the major role in facilitating the segmentation of the Malawi Rift during its opening resulting from extension.

1. Introduction

Recent geological and geophysical studies from the East African Rift System (EARS; Figure 1) highlighted the important and complex role that inherited lithospheric heterogeneity plays in the evolution of largely amagmatic continental rifts. Focusing on the nascent Okavango Rift Zone in northwestern Botswana (Figure 1a), *Leseane et al.* [2015] suggested that the presence of strong lithospheric-scale Precambrian structures could result in extensional strain localization during rift initiation possibly without the assistance of an ascending asthenosphere. *Katumwehe et al.* [2015] used the Miocene Albertine and Rhino grabens in northwestern Uganda (Figure 1a) to suggest that the inherited lithospheric heterogeneity could allow continental rifts to propagate even within the lithosphere of "stable" cratons. Additionally, *Katumwehe et al.* [2015] illustrated how the presence of inherited lithospheric heterogeneity results in strain transfer and rift segmentation in geometrical styles that might not be similar to what is predicted by numerical and scaled models [*McClay and White*, 1995; *McClay et al.*, 2002; *van Wijk*, 2005; *Corti et al.*, 2007; *Aanyu and Koehn*, 2011].

Models of rift segmentation have been highly idealized. One such popular model that has been presented from the EARS, especially Malawi Rift, calls for the segmentation of continental rifts into half-grabens associated with overlapping border faults. These segments are typically ~100 km long, which switch dip polarities from one half-graben to another [*Ebinger et al.*, 1984, 1987; *Rosendahl et al.*, 1992; *Specht and Rosendahl*, 1989]. This study aims at better understanding the geometrical characteristics of continental rift segmentation, its controls and causes, and how these characteristics vary in relation to the temporal development of rifts. The Malawi Rift, which represents the southern part of the Western Branch of the EARS (Figure 1a), is an ideal place for such study because: (1) It is a young rift that displays along-strike segmentation into a number of subbasins. Previous studies suggested the presence of 4 [*Versfelt and Rosendahl*, 1989; *Chorowicz*, 2005], seven [*Specht and Rosendahl*, 1989], 9 [*Rosendahl et al.*, 1992], or 10 [*Ebinger et al.*, 1987] border fault segments along the rift. (2) The rift is developing within Precambrian and Paleozoic-Mesozoic structures with

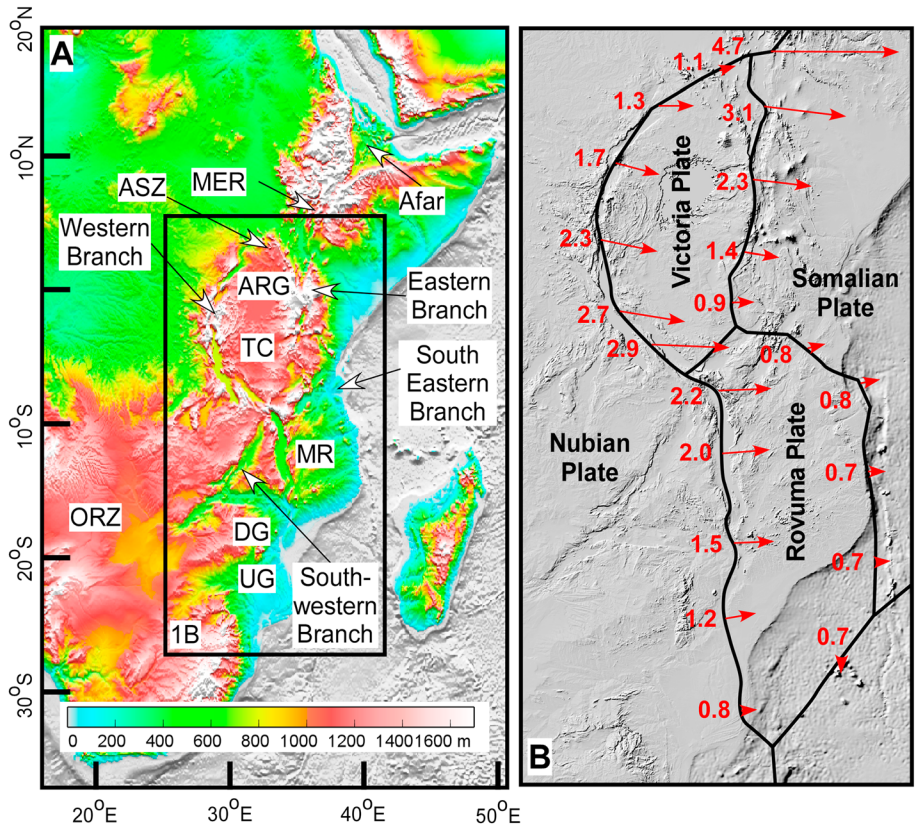

Figure 1. (a) Global 30 arc second elevation data (GTOPO30) DEM showing the East African Rift System (EARS) and the Eastern and Western branches of the EARS. MER = Main Ethiopian Rift. ASZ = Aswa Shear Zone. ARG = Albertine-Rhino Graben. TC = Tanzanian Craton. MR = Malawi Rift. DG = Dombe Graben. UG = Urema Graben. ORZ = Okavango Rift Zone. (B) Red vectors represent surface motions (mm/yr) relative to the Nubian Plate as reported by *Saria et al.* [2014].

different orientations allowing for the examination of the possible influence of preexisting structures on continental rift segmentation. (3) Previous studies suggested that the rift is propagating from north to south with maximum extension rates in the N (Figure 1b) [*Calais et al.*, 2006; *Stamps et al.*, 2008; *Saria et al.*, 2014]. This allows for the evaluation of the temporal evolution of different segments of the rift. The Shuttle Radar Topography Mission (SRTM)-digital elevation model (DEM) aided by few observations from available aeromagnetic data was used to examine the along-strike variability of the Malawi Rift and its segments. Subsequently, along-strike variation in rift segmentation was evaluated in relation to the exposed preexisting structures as well as the southward younging direction of the rift. Our work presents for the first time a detailed segmentation model that differs from previous models in that (1) it divides the Malawi Rift, based on the extent of the rift within different Precambrian terrains, into three sections with different border faults geometries; (2) it shows that the previous models of overlapping half-grabens with alternating opposite polarities can be applied only to the northern section of the Malawi Rift; (3) it shows that continental rifts, as exemplified by the Malawi Rift, can develop across Precambrian terrain boundaries, possibly separating terrains that have different lithospheric structures.

2. The Malawi Rift

2.1. General Description of the Malawi Rift

The Malawi Rift is one of many rift basins of the ~4000 km long EARS (Figure 1a). The EARS begins in the Afar Depression in Ethiopia and trends S as the Main Ethiopian Rift until the NW trending Aswa Shear Zone where it bifurcates into the Eastern and Western branches (Figures 1a and 1b). The two branches wrap around the Tanzanian Craton [*Ring and Betzler*, 1995]. South of the Tanzanian Craton, the Western Branch, continues southeastward following the NW trending structural grain of the Paleoproterozoic Ubendian Belt before approaching the dominantly N-S trending Malawi Rift (Figure 2).

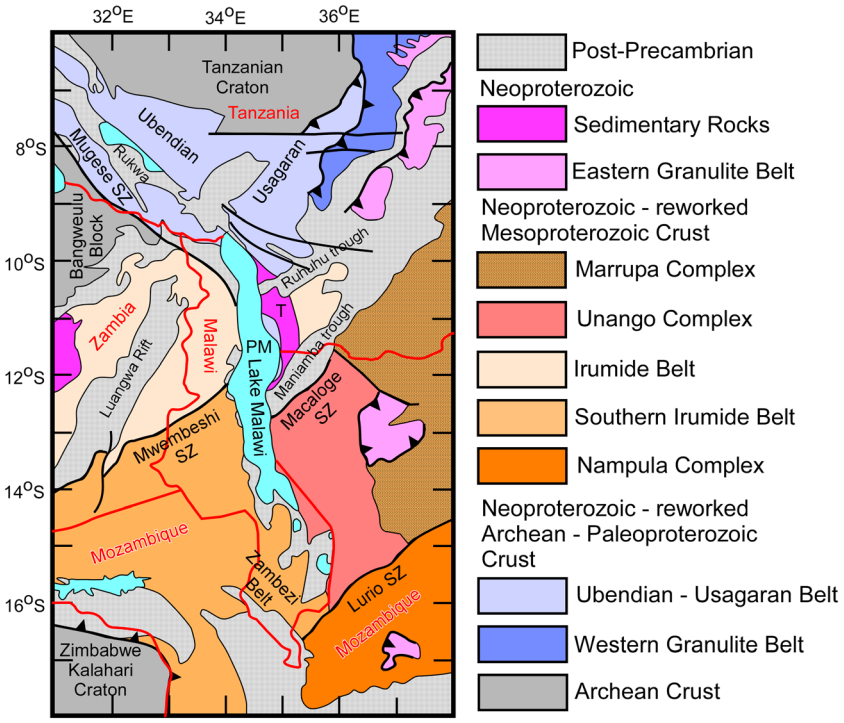

Figure 2. Exposures of Precambrian rocks around the Malawi Rift. Lake Malawi is also known as Lake Nyasi. Modified after *Fritz et al.* [2013]. T = Txitonga Group. PM = Ponta Messuli Complex.

It is suggested that the Malawi Rift continues S for ~900 km from the Rungwe Volcanic Province (the only Cenozoic volcanism associated with the rift) [*Ebinger et al.*, 1989] at its northern tip (Figure 3a), until the Dombe and Urema grabens in Mozambique (Figure 1a) [*Ring et al.*, 1992; *Chorowicz*, 2005]. However, the part of the rift that is filled by Lake Malawi extends for only ~550 km with width ranges between 50 and 75 km (Figure 3a). In the north, the rift strikes N-NW and it is N-NE trending at its southern end (Figures 3a and 3b). In this work, we consider that the Malawi Rift extends from the Rungwe Volcanic Province in the north to the Shire Segment in the south before its termination against the NW trending Shire Graben (Figure 3a).

It is suggested from surface geological observations in its northern part that the Malawi Rift started filling with fluviatile deposits produced from the erosion of Karoo sedimentary rocks before the domination of lacustrine silt deposits when Lake Malawi flooded the rift [*Flannery and Rosendahl*, 1990; *Betzler and Ring*, 1995]. Seismic data suggest that the rift sedimentary fill can reach up to 2 to 3 km thickness in the deepest parts of half-grabens in the northern part of the rift and the rift sedimentary fill becomes thinner southward until it diminishes completely in the Shire Segment where the rift is floored by Precambrian rocks (Figure 3a) [*Specht and Rosendahl*, 1989; *Flannery and Rosendahl*, 1990].

Using constraints from K-Ar and $^{40}Ar/^{39}Ar$ age determination of volcanic rocks, *Ebinger et al.* [1993] concluded that the onset of faulting in the northern part of the Malawi Rift (represented by the Tukuyu-Karonga basin; Figure 3a) started ~8.6 Ma. *Van der Beek et al.* [1998] determined the fission track ages for apatite extracted from Precambrian rock samples collected from the northern part of the Malawi Rift (mostly the Karonga region; Figure 3a). They found the youngest age to be 30 ± 15 Ma. This suggests that either extension localization in the Karonga region of the Malawi Rift started earlier than what has been estimated from the K-Ar $^{40}Ar/^{39}Ar$ age determination or that uplift and denudation might have commenced earlier than rifting. Earlier, *Flannery and Rosendahl* [1990] compared sediments thickness, subsidence, and structural style along the Malawi Rift and concluded that thicker sediments, deeper subsidence, and more structural complexity indicate that the northern part of the Malawi Rift is older than its southern part. Additionally, the observed southward decrease in the amount of basin's subsidence, thickness of the Cenozoic-Quaternary sedimentary rocks, and elevation of the topographic escarpments have been taken as evidence for southward propagation of the rift

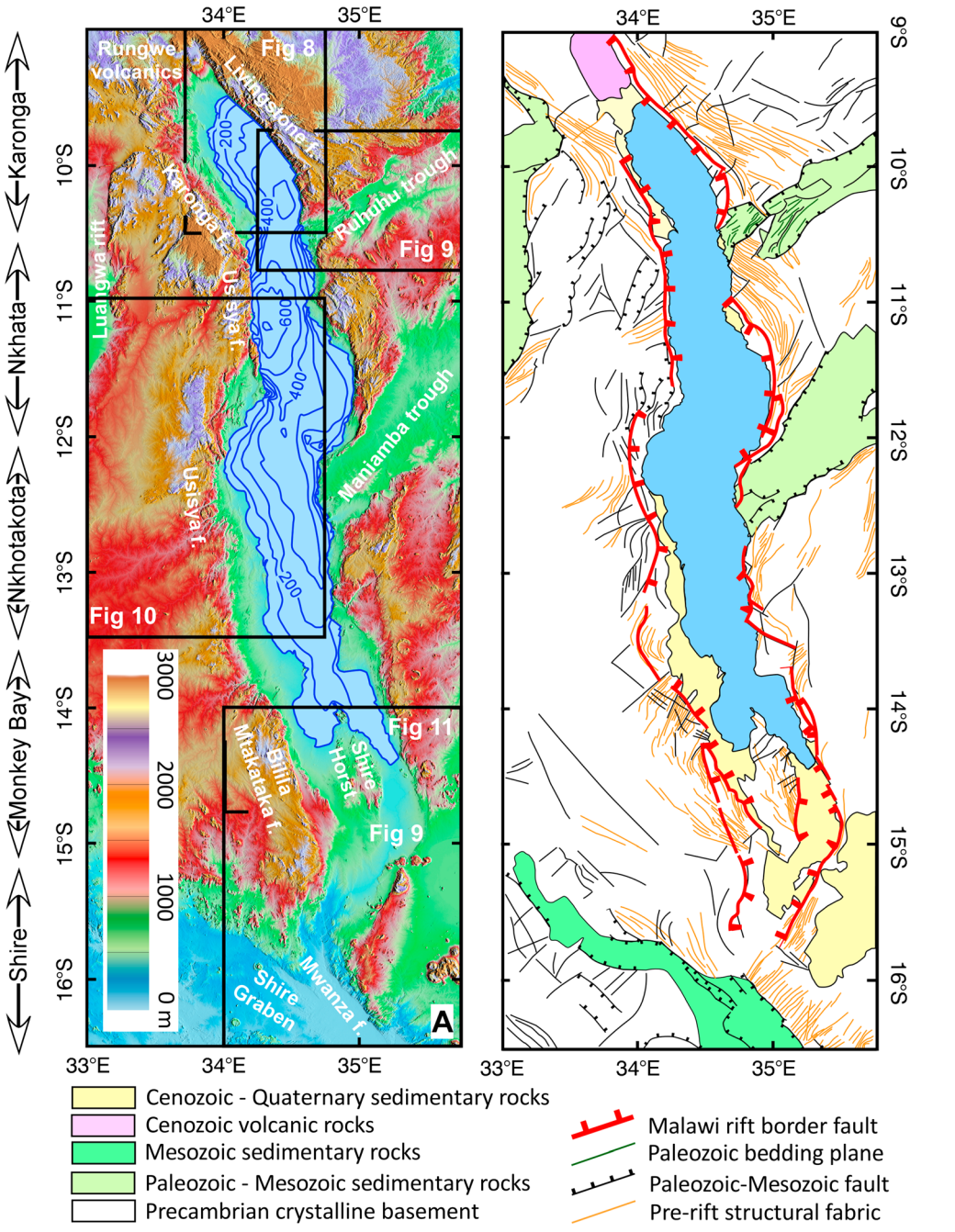

Figure 3. (a) Shuttle Radar Topography Mission (SRTM)-digital elevation model (DEM) of the Malawi Rift. Blue contour lines show water depth within Lake Malawi. Arrows on the left margin of the SRTM DEM shows the extent of the rift segments proposed by *Ebinger et al.* [1984]. (b) Simplified structural map of the Malawi Rift and surroundings. Traces of the Precambrian structural fabric, Paleozoic-Mesozoic faults, Paleozoic bedding planes, and Malawi Rift border faults are extracted from the interpretation of the SRTM DEM. The geographic extent of the Paleozoic is Mesozoic sedimentary rocks, and Cenozoic volcanic rocks are modified from *Chorowicz and Sorlien* [1992].

and its opening in a "zipper-like" fashion from north to south [*Ring and Betzler*, 1995]. *Ebinger et al.* [1987] considered the elevation of the topographic escarpments to be associated with rift-flank uplift.

Based on its geometry, *Ebinger et al.* [1987] divided the Malawi Rift into five broad segments. These are from north to south, Karonga, Nkhata, Nkhotakota, Monkey Bay, and Shire (Figure 3a). The rift is bounded by curvilinear border faults that have, in some places, created topographic escarpments in excess of ~1.5 km (Figure 3a)

[*Ebinger et al*., 1987; *Specht and Rosendahl*, 1989]. The fault throws, which include the topographic escarpment and subsurface extension of the faults, range between ~2.5 km and ~5 km. The most pronounced fault system is the ~120 km long Livingstone Fault located at the northern tip of the eastern side of the rift (Figure 3a). Across the rift, the Karonga Fault extends for 17.8 km to the SE (Figure 3a) [*Biggs et al*., 2010]. This fault is associated with the 2009 earthquake that caused severe damage to the infrastructure of the Karonga region [*Biggs et al*., 2010]. The western side of the center of the rift is deformed by the ~200 km long Usisya Fault (Figure 3a) [*Contreras et al*., 2000]. The Bilila-Mtakataka Fault is ~125 km long and is located at the southwestern end of the rift (Figure 3a) [*Jackson and Blenkinsop*, 1997]. The Shire Segment, in the southern end of the rift, contains the Mwanza Fault (Figure 3a) that is interpreted as a NW striking transcurrent fault [*Castaing*, 1991].

2.2. Kinematics of the Malawi Rift

The current kinematics of the Malawi Rift is largely controlled by E-W extension across the East African Rift System (Figure 1b). Building on previous studies by *Calais et al*. [2006] and *Stamps et al*. [2008], *Saria et al*. [2014] presented a refined kinematic model for the EARS based on Global Positioning System measurements, earthquakes slip vector, spreading rate, and transform fault azimuth data. *Saria et al*. [2014] found that the best fit model of the data used in the study favors an eastward movement of the Rovuma Plate away from the Nubian Plate along the Malawi Rift with the plate's linear velocity decreasing from 2.2 mm/yr in the north to 0.8 mm/yr in the south (Figure 1b).

Although the current kinematics indicate that the Malawi Rift is experiencing orthogonal extension, studies using the geological record suggested that the basin might have experienced oblique rifting in the past. However, the shape of the rift that suggests that it is compartmentalized into a number of left-stepping and NW oriented lens-shaped subbasins, together with the presence of numerous faults within the floor of the rift that are oblique to the general trend of the rift, led to conflicting interpretations of extension obliquity. From seismic data, *Ebinger et al*. [1984] suggested that the rift compartmentalization was due to the presence of NE trending strike-slip faults and that extension is NE-SW, which is oblique to the general north trend of the Malawi Rift, but orthogonal to individual subbasins. *Chorowicz* [1989] used the same seismic data to propose the presence of NW trending transfer faults separating the subbasins, and these faults were developed in association with NW-SE extension. *Chorowicz and Sorlien* [1992] used remotely sensed and field fault slip data to suggest NW-SE extension across the Malawi Rift exerted by the divergence between the Nubian and Somalian (Rovuma) plates in the same direction. Further, *Chorowicz and Sorlien* [1992] interpreted the NW trending Livingstone Fault in the northern tip of the Malawi Rift and the Zambezi Fault (equivalent to Mwanza Fault in Figure 3) in the southern end of the rift as dextral intracontinental transform faults. *Ring et al*. [1992] used remote sensing and field studies to examine cross-cutting relationships between different generations of faults and their slip history in the northern part of the Malawi Rift. *Ring et al*. [1992] proposed a clockwise rotation of the extension direction across the rift. Between 5 and 2 Ma the extension direction was ENE-WSW, and it changed to E-W then NW-SE between 2 Ma and recent times.

2.3. Precambrian Structures Around the Malawi Rift

The Malawi Rift traverses a complex array of Precambrian orogenic belts and Paleozoic-Mesozoic Karoo sedimentary basins (Figures 2 and 3b). The most notable Karoo sedimentary basins around the Malawi Rift are the Luangwa Rift, the Ruhuhu and Maniamba troughs, and the Shire Graben (Figure 3a). In the north, the Malawi Rift strikes NNW, an orientation that is subparallel to the regional structural grain of the Paleoproterozoic Ubendian Belt (Figure 2). This belt was developed at the southwestern margin of the Tanzanian Craton and is characterized by the presence of different crustal blocks separated by NW-trending strike-slip faults [*Fritz et al*., 2013]. In northern Malawi, in the western side of the Malawi Rift, the NW trending Mugese Shear Zone separates the Ubendian Belt from the NE trending Mesoproterozoic Irumide Belt (Figure 2) [*Fritz et al*., 2013]. *Fritz et al*. [2013] suggested that the Paleoproterozoic Ponta Messuli Complex that is exposed on the eastern side of the rift at the Tanzania-Malawi border (Figure 2) might be the southernmost extension of the Ubendian Belt. The Txitonga Group, which is a north trending belt of Neoproterozoic volcano-sedimentary rocks, is exposed to the east of the Ponta Messuli Complex (Figure 2). The presence of bimodal volcanism within this belt has been taken to suggest the presence of a Neoproterozoic rift basin [*Fritz et al*., 2013].

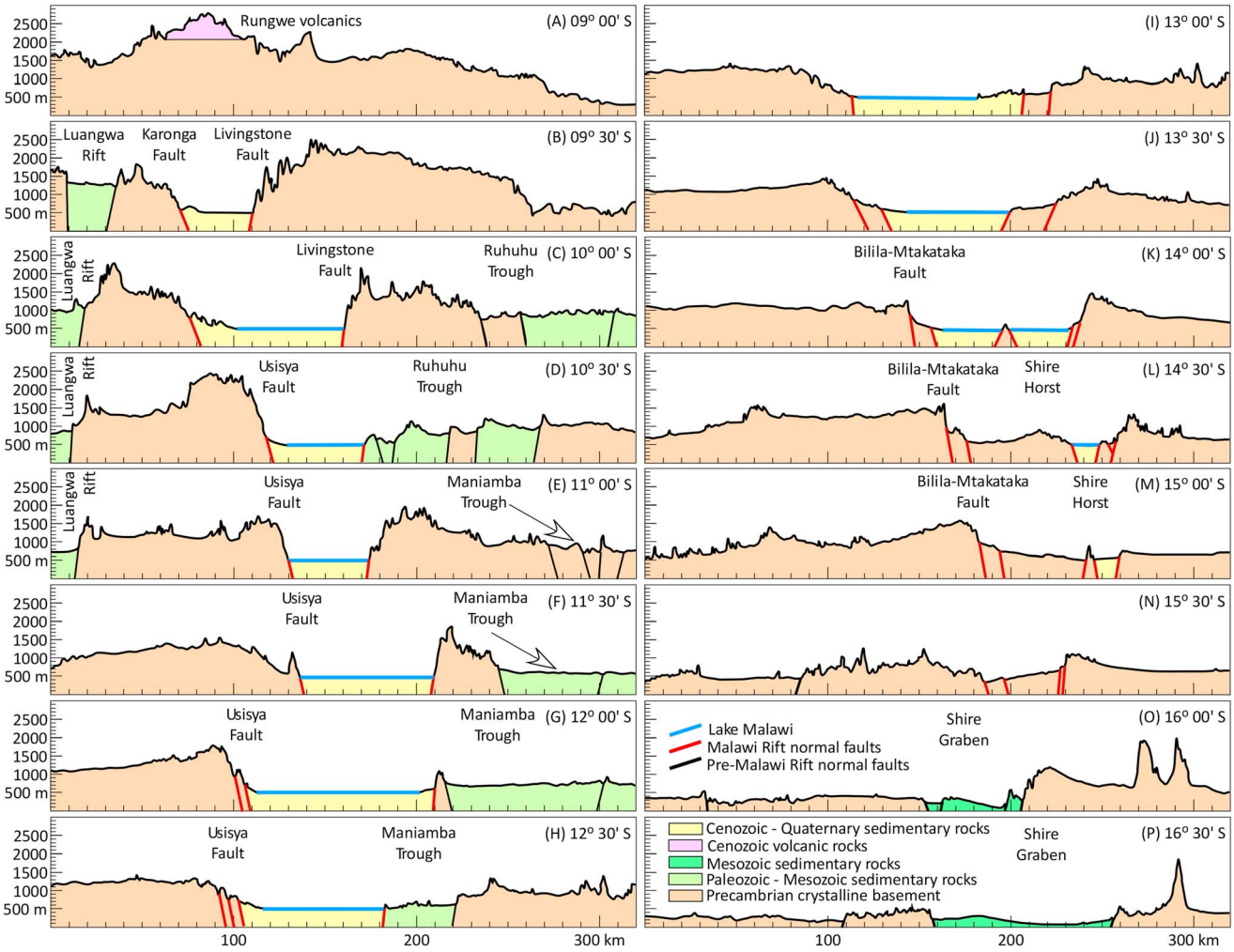

Figure 4. Idealized east-west trending geological sections across the Malawi Rift and surrounding structures spaced at 30′ starting at 9°00′S and ending at 16°30′S. Each profile starts at 33°00′E and ends at 35°45′E. The topographic profiles are extracted from Shuttle Radar Topography Mission (SRTM)-digital elevation model (DEM) with vertical exaggeration of 20. The exposures of the Precambrian crystalline basement, Paleozoic and Mesozoic sedimentary rocks, Cenozoic volcanic rocks and Cenozoic-Quaternary sedimentary rocks as well as the location of pre-Malawi Rift and Malawi Rift normal faults are based on the structural map on Figure 3b.

Unlike its northern part, the southern part of the Malawi Rift extends within Precambrian entities that have regional structural grain, which is not always parallel to the rift itself. This difference seems to coincide with the ENE trending Mwembeshi Shear Zone in southern Zambia and western Malawi and the Macaloge Shear Zone in northwestern Mozambique (Figure 2) [*Bingen et al.*, 2009; *Fritz et al.*, 2013]. The Mwembeshi Shear Zone is considered to mark the boundary between the Irumide Belt in the NW and the Southern Irumide Belt to the SE (Figure 2) [*Fritz et al.*, 2013]. Both belts are Mesoproterozoic in age but differ in that no mid-Mesoproterozoic plutonic rocks are found within the Southern Irumide Belt [*Fritz et al.*, 2013].

The Macaloge Shear Zone is exposed in the southwestern edge of the Karoo Maniamba Trough, and it seems to separate what is the northeastern equivalent of the Southern Irumide Belt in Mozambique from the continuation of the Irumide Belt in southern Tanzania (Figure 2). However, this tectonic relationship remains to be verified because the Precambrian rocks north of the shear zone are buried under the sedimentary rocks of the Maniamba Trough [*Bingen et al.*, 2009] and the continuation of the Irumide Belt into southern Tanzania is not fully confirmed [*Fritz et al.*, 2013].

The Precambrian rocks in the eastern side of the Malawi Rift, south of the Macaloge Shear Zone, have been divided into the Unango, Marrupa, and Nampula complexes, which contain a variety of orthogneisses, and these are over-thrust by the Eastern Granulite Belt (Figure 2) [*Bingen et al.*, 2009]. These continental blocks

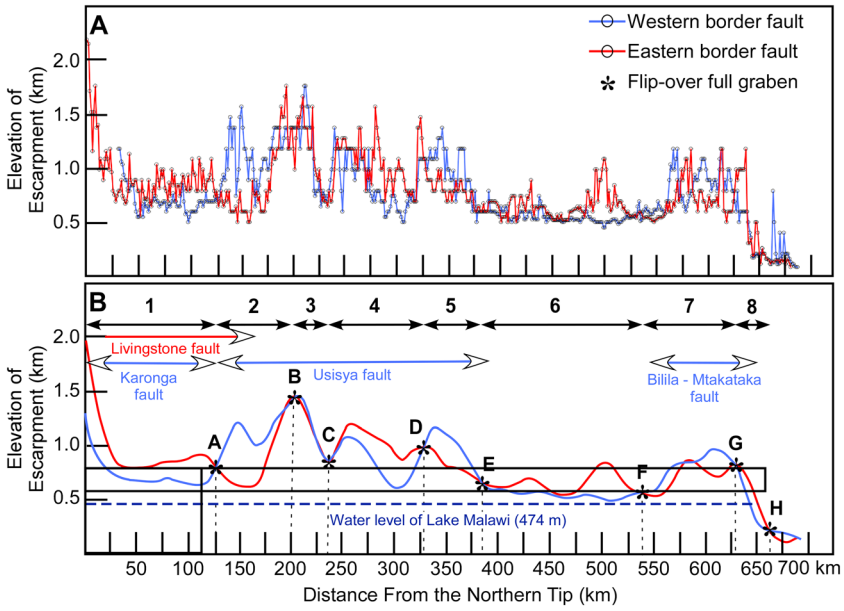

Figure 5. (a) Original data of the displacement profiles of the eastern and western border faults of the Malawi Rift constructed from E-W topographic profiles extracted from Shuttle Radar Topography Mission (SRTM)-digital elevation model (DEM) at 1.4 km spacing starting at 9°30′S and ending at 15°30′S. (B) Smoothing of the original data in Figure 5a using a second-order polynomial fit.

have traditionally been considered to be part of the dominantly Neoproterozoic Pan-African Mozambique Orogenic Belt, which is sandwiched between fragments of East and West Gondwana [*Meert*, 2003]. However, zircon and monazite U-Pb age data suggest the presence of a late Mesoproterozoic crustal component [*Bingen et al*., 2009]. Both *Bingen et al*. [2009] and *Fritz et al*. [2013] suggested that the Unango and Marrupa complexes are the continuation of the Southern Irumide Belt. This implies the absence of a major Precambrian lithospheric boundary under the southern part of the Malawi Rift.

In the southern part of the Southern Irumide Belt close to the Zimbabwe-Kalahari Craton (Figure 2) the structural trend of the Precambrian structures changes from NE to NW. This part of the Southern Irumide Belt has been referred to as the Zambezi Belt [*Hanson et al*., 1994; *Hargrove et al*., 2003]. The NW trend of the Zambezi Belt continues northeastward until the southern part of the Malawi Rift in southern Malawi, where it sharply truncates NE trending Precambrian structure (Figure 3b). Within this region, the NW trending Karoo Shire Graben is also present (Figure 3b). *Chorowicz and Sorlien* [1992] suggested that the rift might have stopped propagating farther south when it encountered these NW trending structures.

3. Data and Methods

In this study, we used SRTM DEM with 90 m spatial resolution to construct E-W topographic profiles at approximately 1.4 km spacing along the entire length of the Malawi Rift. Examples of these profiles, together with geological interpretation for cross-section generation, are shown in Figure 4. The steepest slopes of the profiles are taken to represent the topographic expression of the border faults of the Malawi Rift (Figure 4). In some of the profiles Lake Malawi marks the eastern and western bounds of the rift; hence, the border faults coincide with the shorelines of the lake. However, in other profiles the border faults are found farther east and west of the lake's shorelines (Figure 4). We considered the heights (reliefs above the surface of the lake) of the topographic escarpments to represent the exposed minimum vertical displacement (EMVD) of the border faults. Hence, in order to generate "displacement profiles" for the border faults of the Malawi Rift, we plotted the elevations of the topographic escarpments of the eastern and western border faults as a function of distance of the topographic profiles baselines starting at latitude 9°30′S (Figure 5a). This is because the topographic expression of the northernmost part of the Malawi Rift coincides with this latitude (Figures 3a and 4b). We smoothed the displacement profiles using a second-order polynomial model to minimize the

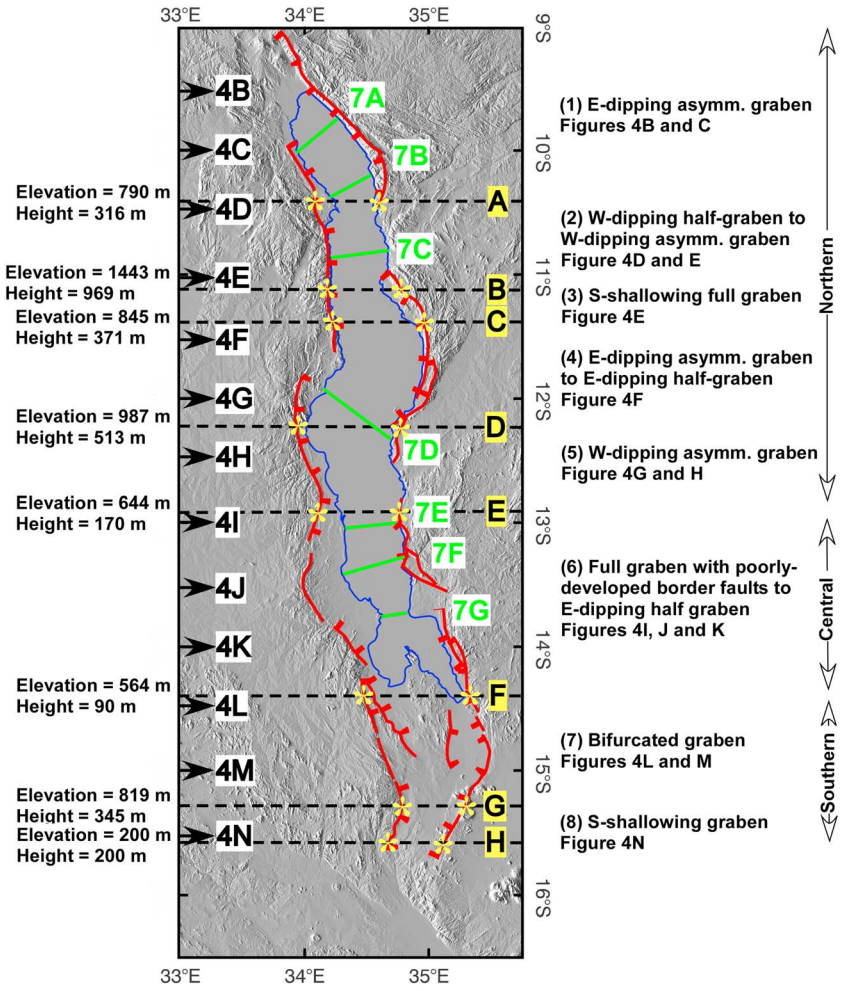

Figure 6. Shuttle Radar Topography Mission (SRTM)-digital elevation model (DEM) of the Malawi Rift showing location and extent of rift segments. Red lines with ticks represent the Malawi Rift border faults. Black arrows with black numbers and letters on white background show the location of geological cross-sections B-N in Figure 4. Dashed black lines with yellow stars and labeled with black letters on yellow background show the location of flip-over full-grabens A-H. Green lines labeled with green numbers and letters on white background show the location of seismic sections A–G in Figure 7.

effect of weathering and erosion that occurred after the formation of the topographic escarpment of the border fault, especially by streams draining into Lake Malawi (Figure 5b).

4. Results: Malawi Rift Segmentation

Along the Malawi Rift, using the displacement profile in Figure 5b, we have established eight rift segments mostly on the basis of along-strike change of the half-graben and asymmetrical graben polarity (Figures 5 and 6). For simplicity, we labeled these segments as Segment 1 to Segment 8. To constrain the extent of each segment we used the positions of what we refer to as the "flip-over full-graben." The locations of these flip-over full-grabens are shown with black stars in Figure 5b and yellow stars in Figure 6, and these are labeled A to H. We define the flip-over full-graben as a graben in which, regardless of its amount, the EMVD on both border faults is equal and that this graben separates half-grabens or asymmetrical grabens of opposite polarities. The amounts of the EMVD (labeled as height) on the border faults of the flip-over full-graben are shown in Figure 6. We did not find any systematic along-strike change in the geometry of the flip-over full-grabens such as a decrease from north to south in the amount of EMVD. For example, we found that the EMVD on the border faults of the northernmost flip-over full-graben (graben "A") to be 316 m, and it is 345 m in the graben just north of the southernmost flip-over full-graben (graben G; Figure 6). Between the two, the EMVD varies unsystematically between 969 and 90 m.

Below, we describe the geometrical characteristics of each segment in terms of their formation as a half-graben, asymmetrical graben, or full-graben. We reserve the use of the term full-graben to a rift where the EMVDs are equal in both border faults. Differently, we use the term half-graben when the EMVD is accommodated in only one border fault where the opposite margin of the rift acts as a hinge zone. In this case, we define the polarity of the half-graben with the side in which the border fault is located and the inferred dip direction of the rift-filling sediments. For example, an east dipping half-graben will have its border fault in its eastern side, and the rift-filling sediments are inferred to dip to the east. Finally, we use the term asymmetrical graben to any basin with EMVD greater in one border fault compared to the other. Similar to the way we define the polarity of half-grabens, we define the polarity of the asymmetrical graben with the side of the border fault with the greater EMVD and the inferred dip direction of the rift-filling sediments. For example, a west dipping asymmetrical graben is a graben where the border fault on its western side has the greater EMVD and that the rift-filling sediments are inferred to be dipping to the west.

4.1. Segment 1: East Dipping Asymmetrical Graben

Segment 1 is the northernmost segment of the Malawi Rift (Figure 6). It extends for ~125 km in a NNW-SSE direction from the Rungwe Volcanic Province to the northern intersection of the Malawi Rift with the Ruhuhu Trough (Figure 3a). This segment is an east dipping asymmetrical graben, in which the EMVD of the eastern border fault represented by the Livingstone Fault is consistently higher than that of the western border fault represented by the Karonga Fault (Figure 5). In the northern part of this segment, a topographic escarpment reaching 2000 m defines the Livingstone Fault, while the Karonga Fault has an escarpment with 1200 m elevation; hence, the difference between the two escarpments is 800 m (Figure 5). Taking the elevation level of Lake Malawi to be 474 m, the EMVD can be estimated to be 1526 m in the Livingstone Fault and 726 m in the Karonga Fault. The elevations on both escarpments decrease abruptly to the south in a 25 km distance from the site of maximum EMVD reaching 800 m for the Livingstone Fault and 650 m for the Karonga Fault, hence reducing the difference in the EMVD between the two border faults to only 150 m (Figure 5b). For ~100 km farther south, until close to the southern end of Segment 1, the EMVD on both border faults is generally uniform averaging 800 m for the Livingstone Fault and 650 m for the Karonga Fault (Figure 5). At the end of the segment the elevation of the Livingstone Fault escarpment drops while that of the Karonga Fault elevates ending with the two escarpments reaching the same elevation at 790 m, hence forming a flip-over full-graben with an EMVD of 316 m in both border faults (Figure 6).

On the surface, the east dipping asymmetrical graben geometry of Segment 1 with a decreased difference in EMVD of border faults from north to south is best exemplified by the geological cross sections in Figures 4b and 4c. At the subsurface, Segment 1 of the Malawi Rift displays similar east dipping asymmetrical graben geometry as indicated by the interpretation of seismic sections from *Specht and Rosendahl* [1989] (Figures 7a and 7b).

4. 2. Segment 2: West Dipping Half-Graben to West Dipping Asymmetrical Graben

Segment 2 extends for ~75 km within the zone where the Malawi Rift intersects the Ruhuhu Trough (Figure 3a). In the first 50 km south of flip-over full-graben "A" this segment is largely a west dipping half-graben with significant EMVD in the western border fault represented by the Usisya Fault, whereas the eastern side of the rift, for the most part, represents a hinge zone (Figure 6). In this part of the segment the elevation of the Usisya Fault escarpment increases to reach 1200 m whereas the eastern escarpment decreases in elevation to reach a minimum of 550 m. This corresponds to EMVD of 726 m in the western border fault and only 76 m in the eastern side of the rift. Farther south of the west dipping half-graben the topographic escarpment of both border faults rises sharply to form a west dipping asymmetrical graben with a southward diminishing asymmetry until reaching a flip-over full-graben with border faults escarpment elevation of 1443 m, hence a EMVD of 969 m. This flip-over full-graben represents the second deepest surface expression of the Malawi Rift after the Livingstone Fault escarpment.

The surface expression of the west dipping half-graben geometry of Segment 2 is best exemplified by the geological cross sections in Figure 4d. Also, the geometry of the flip-over full-graben is best represented by the cross section in Figure 4e. At the subsurface, similar west dipping half-graben geometry is observed from the interpretation of the seismic sections of *Specht and Rosendahl* [1989] (Figure 7c). However, the surface and the subsurface cross sections differ in that the seismic data show the western border fault of the half-graben to be under Lake Malawi rather than under the topographic escarpment.

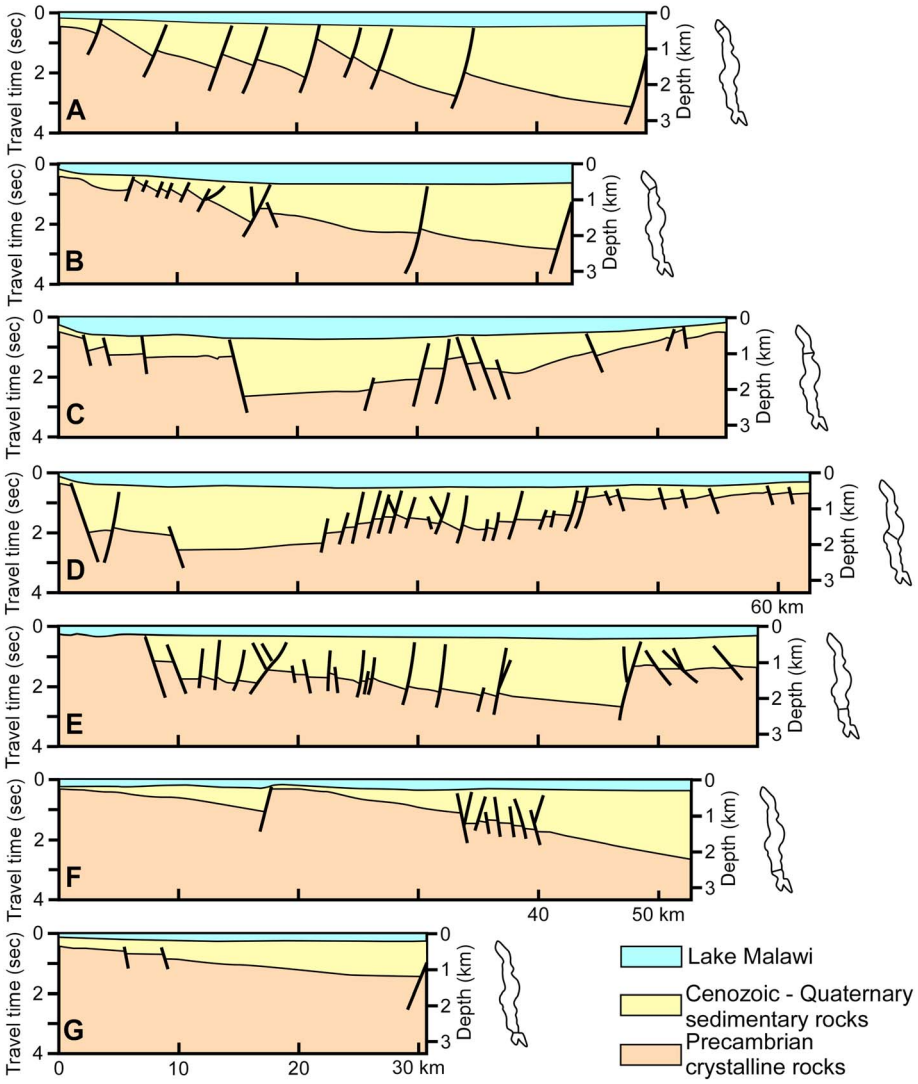

Figure 7. Line interpretation of selected seismic sections of *Specht and Rosendahl* [1989] across Lake Malawi. See Figure 6 for seismic sections location.

4.3. Segment 3: South Shallowing Full-Graben

Segment 3 extends for only ~35 km in a NNW-SSE direction, and it consists of a full-graben which shallows to the south (Figure 5). South of the flip-over full-graben "B," where the EMVD on both border faults is 969 m, the graben becomes consistently shallower until the EMVD reaches 371 m at the end of the segment as marked by flip-over full-graben "C" (Figures 5 and 6). The western border fault of the graben is represented by the southern continuation of the Usisya Fault, whereas the eastern border fault is represented by a curvilinear escarpment that follows closely the structural trend of the Paleoproterozoic Ponta Messuli Complex, which represents the southernmost extension of the Ubendian Belt (Figures 2 and 3b).

4.4. Segment 4: East Dipping Asymmetrical Graben to East Dipping Half-Graben

Segment 4 extends for ~92 km in a NNE-SSW direction starting as an east dipping asymmetrical graben where the EMVD on the eastern border fault is higher than that of western border fault (Figure 5). The elevation of the escarpments of the western border fault, represented by southern continuation of the Usisya Fault, drops from 1100 m at its highest point to 600 m at the southern end of the segment. This corresponds to a decrease of the EMVD from 626 m to 126 m. In the east, the elevation of the eastern escarpment drops from 1200 m in the northern part of the segment to 900 m in its southern part,

corresponding to EMVD of 726 and 426 m, respectively. This results in a gradual change of Segment 4 from an east dipping asymmetrical graben in the north to an east dipping half-graben to the south. The east dipping asymmetrical graben geometry of Segment 4 is illustrated by the geological cross-section in Figure 4f.

4.5. Segment 5: West Dipping Asymmetrical Graben

Segment 5 stretches for 58 km in a N-S direction as a dominantly west dipping half-graben. At its highest point, the escarpments of the western border fault represented by the southern continuation of the Usisya Fault reached 1200 m before dropping to 600 m at the southern end of the segment (Figure 5) producing EMVD of 726 m and 126 m, respectively. To the west, the escarpments of the western border fault drops from 1000 m in the northern part of the segment to 600 m at its southern end resulting in EMVD of 526 m and 126 m, respectively.

The surface geometry of the west dipping asymmetrical graben geometry of this segment is best represented by the geological cross-sections in Figures 4g and 4h. At the subsurface, similar west dipping asymmetrical geometry is observed from the interpretation of the seismic section of *Specht and Rosendahl* [1989] (Figure 7d).

4.6. Segment 6: Full-Graben With Poorly Developed Border Faults to East Dipping Half-Graben

Segment 6 is the longest segment in the Malawi Rift extending for 153 km in a NNW-SSE direction. This segment, in its northern part, is dominated by a shallow full-graben with poorly developed border faults represented by topographic escarpments ranging between 500 and 700 m (Figure 5), hence EMVD of only 26 m and 226 m, respectively. However, in places especially in the southern part of the segment, the escarpment of the eastern border fault becomes more prominent reaching an elevation of 800 m resulting in the transitioning of the segment from shallow full-graben to an east dipping half-graben with an EMVD of 326 m on the eastern border fault.

The shallow full-graben nature of this segment is clearly illustrated in the cross-sections in Figures 4i and 4j. At the subsurface, similar geometry of a full-graben with poorly developed border fault is observed from the interpretation of the seismic section of *Specht and Rosendahl* [1989] (Figure 7e). This seismic section shows that the northern part of Segment 6 is dominated by a graben that is dissected by numerous normal faults at its floor (Figure 7e). Differently, the surface expression of the east dipping half-graben geometry of the southern part of Segment 6 is shown in the cross-section of Figure 4k. The east dipping half-graben geometry of this part of Segment 6 is also observed from the subsurface as indicated by the interpretation of the seismic sections of *Specht and Rosendahl* [1989] (Figures 7f and 7g).

4.7. Segment 7: Bifurcated Graben

Segment 7 extends for 89 km in a NNW-SSE direction, and it is characterized by the gradual rise of the topographic escarpment of the border faults of the Malawi Rift reaching 950 m in the west represented by the Bilila-Mtakataka Fault and 850 m in the east (Figures 3 and 5). This corresponds to EMVD of 476 m and 376 m, respectively. Here the Malawi Rift is bifurcated into an eastern and a western graben separated by the NNW-elongated Shire Horst (Figure 3). The eastern graben seems to be narrower (~20 km), deeper, and filled with Cenozoic-Quaternary sedimentary rocks, whereas the western graben is wider (~50 km), shallower, and floored with rocks of the Mesoproterozoic Southern Irumide Belt. The geometry of Segment 7 is best exemplified by the geological cross-sections in Figures 4l and 4m.

4.8. Segment 8: South Shallowing Graben

In Segment 8, the Malawi Rift changes its orientation from NNW trending to NE trending forming a full-graben that shallows to the SW (Figure 5). The topographic escarpments of both border faults drop sharply from 800 m in the north to 200 m to the south within the 35 km length of the segment (Figure 5). We did not use the level of Lake Malawi as a datum to estimate the EMVD because this segment is outside the lake with topography that slopes down to SW reaching close to zero m elevation in the Shire Graben. Instead of the lake level, we used the relatively flat floor of the Malawi Rift as a datum. Segment 8 of the Malawi Rift is floored by the rocks of the Mesoproterozoic Southern Irumide Belt. The geometry of Segment 8 is exemplified by the cross-section in Figure 4n.

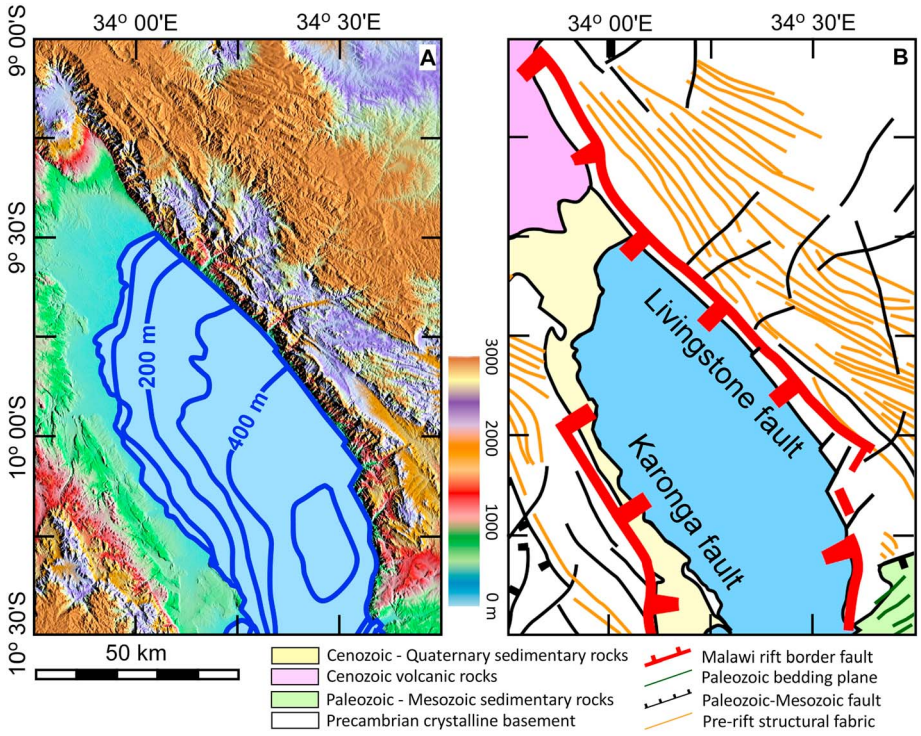

Figure 8. (a) Shuttle Radar Topography Mission (SRTM)-digital elevation model (DEM) of the northern part of the Malawi Rift. Blue contour lines show water depth within Lake Malawi. (b) Simplified structural map of the northern part of the Malawi Rift. Traces of the Precambrian structural fabric, Paleozoic-Mesozoic faults, Paleozoic bedding planes, and Malawi Rift border faults are extracted from the interpretation of the SRTM DEM. The geographic extent of the Paleozoic and Mesozoic sedimentary rocks and Cenozoic volcanic rocks is modified from *Chorowicz and Sorlien* [1992]. See Figure 3 for location.

5. Discussion

5.1. Influence of Inherited Lithospheric Heterogeneity

In this section, we discuss the relationship of the preexisting structures to the border faults and grabens in different segments of the Malawi Rift.

We suggest that the development of Segment 1 of the Malawi Rift, in regards to orientation and geometry, has been greatly influenced by the structural grain of the Paleoproterozoic Ubendian Belt, especially the NW trending Mugese Shear Zone (Figure 2). This orogenic belt has prominent NW trending preexisting structures (in the form of penetrative transcurrent shear fabric and zones of Proterozoic cataclasites) [*Ring et al*., 2002] favoring strong extensional strain localization during rifting allowing the Livingstone Fault to develop as the eastern border fault of the rift with considerable EMVD (Figure 8). Similarly, the NW trending structure of the Mugese Shear Zone provided the upper level lithospheric heterogeneity to extensional strain localization leading to the development of the Karonga Fault as the western border fault of this segment (Figure 8).

In Segment 2, our observations suggest that the presence of the Ruhuhu Trough played an important role in its development as a west dipping half-graben in the N part of the segment, which transitioned into west dipping asymmetrical graben to the south. At its intersection with the Malawi Rift, the northern half of the Ruhuhu Trough is filled with Paleozoic sedimentary rocks with bedding planes at high angle to the rift and this gives place farther south to exposures of the Neoproterozoic Txitonga Group with NNW trending structural grain (Figures 2, 3b, and 9). This might have prevented the development of an eastern border fault in the northern part of the segment where the Paleozoic sedimentary rocks are exposed, but the EMVD gradually increased to the south facilitated by the presence of the NNW tending structures of the Txitonga Group.

Our data suggest that the development of Segment 4 as an east dipping asymmetrical graben in the north transitioning into an east dipping half-graben to the south is largely due to the presence of the

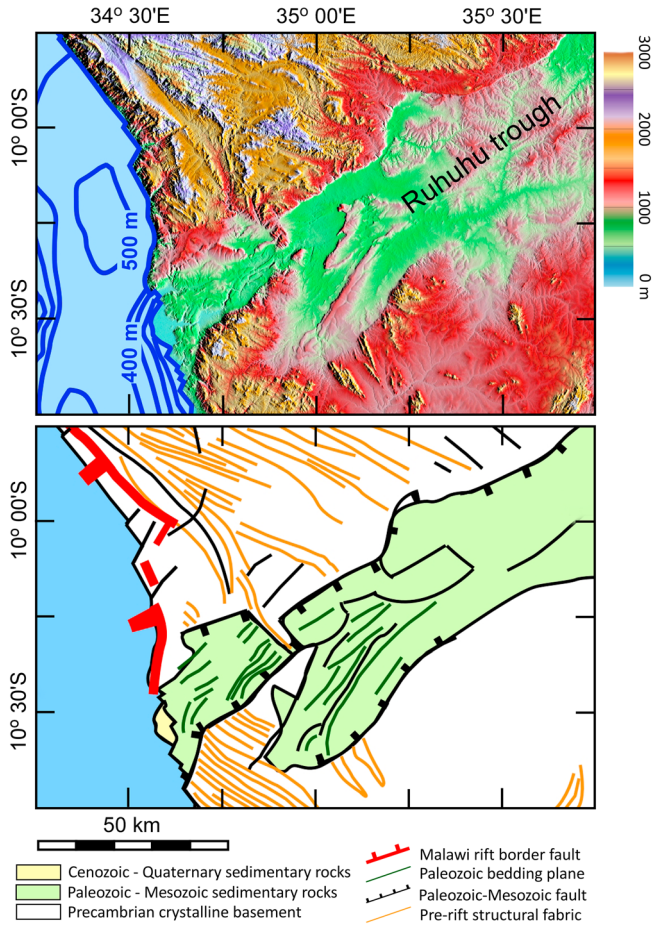

Figure 9. (a) Shuttle Radar Topography Mission (SRTM)-digital elevation model (DEM) of the Malawi Rift at its intersection with the Ruhuhu Trough. Blue contour lines show water depth within Lake Malawi. (b) Simplified structural map of the Malawi Rift at its intersection with the Ruhuhu Trough. Traces of the Precambrian structural fabric, Paleozoic-Mesozoic faults, Paleozoic bedding planes, and Malawi Rift border faults are extracted from the interpretation of the SRTM DEM. The geographic extent of the Paleozoic and Mesozoic sedimentary rocks is modified from *Chorowicz and Sorlien* [1992]. See Figure 3 for location.

Paleoproterozoic Ponta Messuli Complex with well-developed north trending fabric (represented by faults bounding the complex and regional metamorphic foliation) [*Bingen et al.*, 2009] that facilitated strain localization in the eastern border fault of this segment of the Malawi Rift (Figures 2 and 3b).

In contrast, the presence of the Maniamba Trough played an important role in the development of Segment 5 as a west dipping asymmetrical graben. At its intersection with the Malawi Rift, the Maniamba Trough is filled with Paleozoic sedimentary rocks with bedding planes at high angle to the Malawi Rift (Figure 3a). This prevented the development of an eastern border fault in the segment.

The striking change in the geometry of the Malawi Rift from dominantly asymmetrical grabens and half-grabens in the N with alternating polarity (Segments 1–5) to a broad and shallow graben with poorly developed border faults in the south coincides with a number of Precambrian geological features. This change seems to occur south of the Mwembeshi and Macaloge shear zones that separates the Mesoproterozoic Irumide Belt in the north from the Southern Irumide Belt and the Unango and Marrupa complexes to the south (Figure 2). The Mwembeshi Shear Zone appears to be a prominent structure as suggested by its magnetic signature (Figure 10). Here the Precambrian fabric shows prominent NE trending structures that truncate east trending structures to the north from NE trending structures to the south. Although the Irumide Belt is exposed in the western part of the Malawi Rift, much of the northern part of the rift extends within the Paleoproterozoic Ubendian Belt, its southern continuation the Ponta Messuli Complex and the Neoproterozoic Txitonga Group (Figure 2). The regional fabric in these Precambrian terrains is dominantly subparallel to the extent of the Malawi Rift (see Figure 8 as an example). Differently, the structural grain in the Southern Irumide Belt in the western part of Segment 6 of the Malawi Rift is dominantly at high angle to the rift's trend (Figure 3b). The trend of the Precambrian structures in the Unango Complex SE of the Macaloge Shear Zone (in the northern part of Segment 6) is also at high angle to the general north trend of the Malawi Rift (Figures 2 and 3b). The orientation of these preexisting structures is unfavorable for extensional strain localization; this might have prevented the development of border faults in the entire western side of Segment 6 and the northern part of the eastern side of the segment. A better developed eastern border fault is found in the southern part of Segment 6 where the Precambrian structures assumed north trend, hence allowing for extensional strain localization during extension.

The change of orientation of the Malawi Rift from NNW trending in Segment 7 to NE trending in Segment 8 is largely controlled by the structures of the Mesoproterozoic-Neoproterozoic Southern Irumide Belt (Figure 2). These structures form upper level lithospheric heterogeneity clearly apparent from its magnetic signature

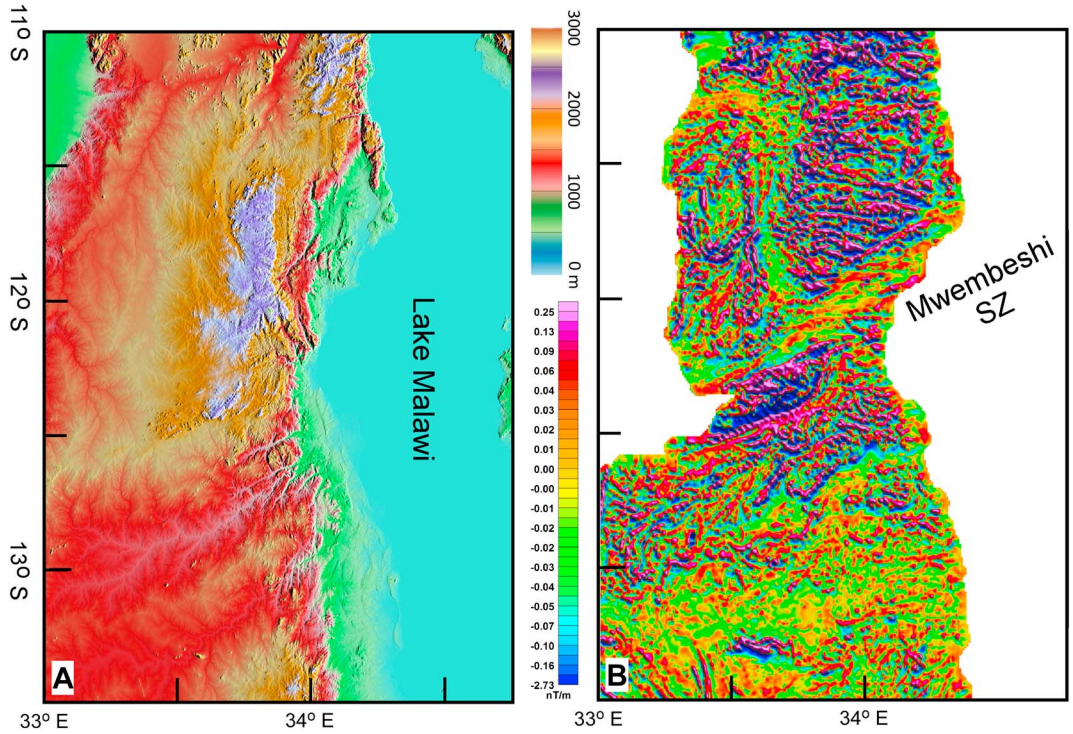

Figure 10. (a) Shuttle Radar Topography Mission (SRTM)-digital elevation model (DEM) of the Malawi Rift at its intersection with the Mwembeshi Shear Zone. (b) Aeromagnetic image of the Malawi Rift at its intersection with the Mwembeshi Shear Zone created from the vertical derivative. See Figure 3 for location. The aeromagnetic data used were acquired by the Government of Malawi between 1984 and 1985 with 12 m altitude E-W flight paths oriented and line spacing of 1 km and 10 km tie lines, with terrain clearance of 120 m.

(Figure 11). These structures change from NNW trending within Segment 7 to NE trending within Segment 8 (Figure 11). Farther south, the NE trending structures of the Mesoproterozoic Southern Irumide Belt are sharply truncated by the NE trending structures of the Neoproterozoic Zambezi Belt, which seem to have provided preexisting lithospheric heterogeneity for extensional strain localization during the formation of the Mesozoic Shire Graben (Figure 11). The topographic expression of the Malawi Rift is not recognizable after it encounters the NW trending Zambezi Belt and Shire Graben (Figure 11).

5.2. Hierarchical Segmentation of the Malawi Rift

Our results reveal a previously unrecognized pattern of the Malawi Rift, in which 8 segments were identified on the basis of morphological expression of the border faults of the rift (Figures 5 and 6). However, a higher order of rift segmentation can be established on the basis of the influence of the inherited lithospheric heterogeneity on the evolution of the rift. Hence, we suggest describing the segmentation of the Malawi Rift as a first-order and second-order rift segmentation.

5.2.1. First-Order Segmentation of the Malawi Rift

By considering the first-order rift segmentation, we propose dividing the Malawi Rift into Northern, Central, and Southern sections (Figure 6). The Northern Section encompasses segments 1 to 5 and stretches dominantly parallel to the structural grain of the Paleoproterozoic Ubendian Belt and the Ponta Messuli Complex, and the Neoproterozoic Txitonga Group (Figures 2 and 6). These Precambrian terrains are characterized by the presence of NNW to NW trending fabrics mostly developed in association with lithospheric-scale shear zones such as the Mugese Shear Zone (Figure 2) [*Fritz et al.*, 2013]. Additionally, the presence of bimodal volcanism in the Txitonga Group has been interpreted as an indication of possible Neoproterozoic rift site [*Fritz et al.*, 2013]. Hence, we suggest here that the inherited Precambrian lithospheric heterogeneity in the Northern Section of the Malawi Rift provided favorable preexisting structural orientation that can facilitate strain localization during orthogonal (E-W) or oblique (NE-SW or NW-SE) extension.

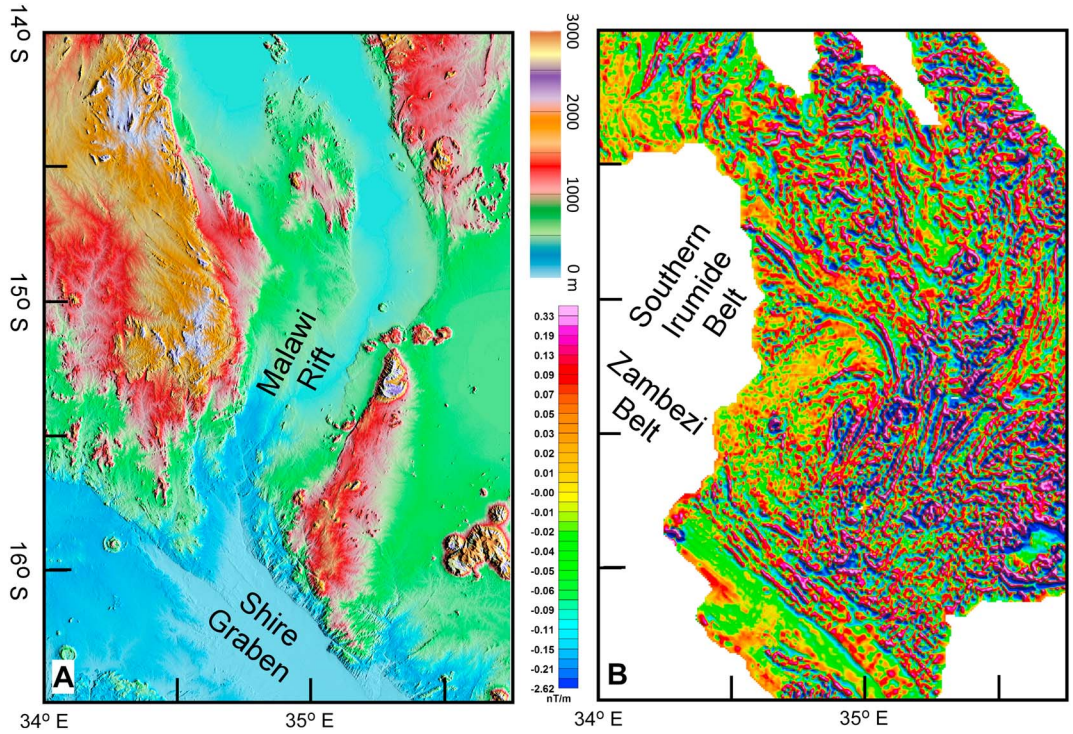

Figure 11. (a) Shuttle Radar Topography Mission (SRTM)-digital elevation model (DEM) of the southern part of the Malawi Rift. (b) Aeromagnetic image of the southern part of the Malawi Rift created from the vertical derivative. See Figure 3 for location. The specification of the aeromagnetic data is that as data in Figure 10b.

The Central Section of the Malawi Rift comprises Segment 6, and it extends within the Mesoproterozoic-Neoproterozoic Southern Irumide Belt and Unango Complex. Its boundary with the Northern Section closely coincides with the ENE trending Mwembeshi and Macaloge Shear Zones (Figures 2 and 6). The Malawi Rift in this section largely extends within Precambrian structural grain that does not favor significant influence of inherited lithospheric heterogeneity in strain localization during rifting. The Precambrian entities in this section either have regional structural trend that is oblique to the Malawi Rift or lack the presence of penetrative structures (Figure 10b). Nonetheless, the presence of this section of the rift between what has been mapped as different Precambrian terrains (Southern Irumide Belt in the W and the Unango Complex to the east) is tempting to consider the possible presence of a Precambrian terrain boundary beneath this section of the Malawi Rift. However, the lithological and age similarity between the Southern Irumide Belt and the Unango Complex, where both are late Mesoproterozoic gneisses that were reworked during the Neoproterozoic [*Bingen et al.*, 2009; *Fritz et al.*, 2013], makes this scenario less likely. Nonetheless, more geophysical studies are needed to test the possibility of the presence of a Precambrian suture beneath the Central Section of the Malawi Rift. Until then, we propose that the lack of strong inherited lithospheric heterogeneity that is needed to assist in strain localization during extension might have resulted in the development of the Central Section of the Malawi Rift as a full-graben with poorly developed border faults and highly dissected floor (Figures 4i–4k and 7e).

The Southern Section of the Malawi Rift constitutes Segments 7 and 8, and it extends within the Mesoproterozoic-Neoproterozoic Southern Irumide Belt before it terminates against the NW trending Neoproterozoic Zambezi Belt and the Mesozoic Shire Graben (Figures 3 and 11). This section of the rift curves and narrows south of Lake Malawi from a NW trend in the N to a NE trend in the south (Figure 11). Here the rift is dominantly floored by Mesoproterozoic-Neoproterozoic rocks of the Southern Irumide Belt, suggesting the lack of any significant sedimentation-related subsidence. The sharp difference between the Central and the Southern sections of the Malawi Rift is that the latter is underlain by the portion of the Southern Irumide Belt, where strong NW and NE trending regional fabric is present (Figure 11b). In the Southern Section, the curvilinear trace of the

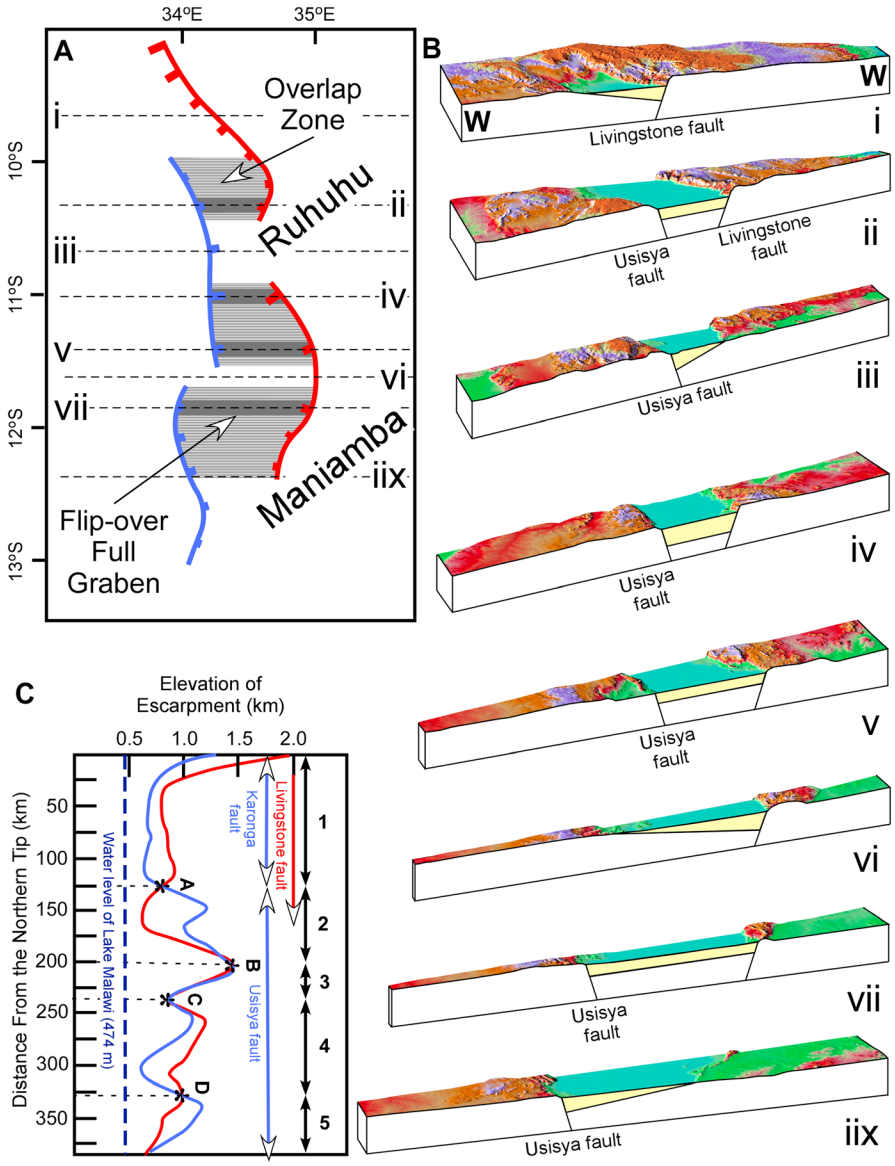

Figure 12. An idealized model of the northern region of the Malawi Rift showing along-strike half-graben polarity alternation form east dipping to west dipping with full-grabens occupying the overlap zones between the eastern and western border faults. The numbers i–iix corresponds to the locations of the slices in Figure 12b. (b) Three-dimensional perspective views of different slices of the northern part of the Malawi Rift. The horizontal surface views are created from the Shuttle Radar Topography Mission (SRTM)-digital elevation model (DEM) in Figure 3a. The cross-section views are idealized from the geological cross sections in Figure 4. (c) Displacement profiles of the eastern and western border faults of the Northern Section of the Malawi Rift constructed from E-W topographic profiles extracted from SRTM DEM at 1.4 km spacing starting 9°30′S and ending at 13°00′S. The original data were smoothed using second-order polynomial fit.

rift impressively follows the trend of the Precambrian structures (Figures 11a and 11b). Hence, we propose that the presence of inherited lithospheric heterogeneity in the form of shear zones and metamorphic foliation has assisted strain localization during extension, especially E-W extension. Additionally, the presence of the NW trending Mwanza Fault at the southern end of the Malawi Rift that has been interpreted as intra-continental transform fault [*Chorowicz and Sorlien*, 1992] and the apparent dextral offset of the Mwembeshi and Macaloge Shear Zones, which have been interpreted as a once continuous prerift structures [*Ring et al.*, 2002; *Fritz et al.*, 2013], favors NW-SE oblique extension, at least at some stage of the rift evolution. Such NW-SE extension will result in a significant dextral strike-slip component within Segment 7, which has a NW

trend as well as other NW trending segments of the rift. The lack of sedimentation-related subsidence might be due to a combination of the presence of the inherited lithospheric heterogeneity that has localized extension in the uppermost part of the lithosphere coupled with the diminishing extension across the rift (Figure 1b).

5.2.2. Second-Order Segmentation of the Malawi Rift

Our results suggest that the Northern Section of the Malawi Rift experienced second-order segmentation through the alternation of half-grabens or asymmetrical grabens of opposite polarities separated by overlap zones that host flip-over full grabens (Figures 12a–12c). This segmentation is similar to what has been proposed by *Ebinger et al*. [1987] for the northern part of the Malawi Rift, where four segments were identified. However, we restrict the second-order segmentation pattern to only the Northern Section of the Malawi Rift. We note that the change of polarity of the asymmetrical graben or half-grabens in the Northern Section coincides with regions where the Paleozoic-Mesozoic Ruhuhu and Maniamba troughs are found in the eastern side of the Malawi Rift at high angle to its general N-trend (Figures 3 and 12a). These Paleozoic-Mesozoic grabens were able to modify the strain field in the upper crust, hence facilitating second-order segmentation of border faults, and they do not seem to have been reactivated by the Cenozoic rifting event [*Rosendahl et al*., 1992].

Based on the classification of *Morley et al*. [1990], the second-order segmentation of the Northern Section of the Malawi Rift can be described as "conjugate convergent overlapping" because of the geometrical relationship between the border faults. Idealizing the border faults in the Northern Section suggests the presence of four ~150 km long alternating border faults that dip toward each other (Figure 12a). These alternating border faults enclose overlap zones with length to width ratios close to one (Figure 12a). The border faults overlapping pattern of the Northern Section is distinct from other border fault linkage patterns such as the "conjugate convergent approaching" [*Morley et al*., 1990], where the overlap length to overlap width ratio is zero.

5.3. Kinematics of the Malawi Rift and Rift Segmentation

It is observed that the linear velocity of the movement of the Rovuma Plate relative to the Nubian Plate decreases from 2.2 mm/yr in the northern part of the Malawi Rift to 1.5 mm/yr in its southern part (Figure 1b) [*Saria et al*., 2014]. Also, it is observed that there is a general southward decrease in the elevation of the topographic escarpments of the Malawi rift [*Ring and Betzler*, 1995]. Both observations are indications of southward propagation of the rift. Our work agrees with the observation that there is a general southward decrease in the elevation of the topographic escarpment that we used as a proxy for the EMVD (Figure 5) However, we argue that there is no systematic correlation between the southward propagation of the Malawi Rift and the spatial extent and geometry of its segments: (1) We did not observe any systematic decrease from north to south in the elevations of the flip-over full grabens or their EMVD (Figure 5). With the exception of graben "B" and "H" all other grabens are found within elevations ranging between 600 and 1000 m (Figure 5). (2) We did not find any change in the length of border faults or the geometry of overlap zones forming the second-order rift segmentation of the Northern Section of the Malawi Rift (Figure 12a). All four border faults are ~150 km long and the enclosed overlap zones have length to width ratios of about one. (3) The width of the rift in its entire length is uniform with changes that can be largely attributed to facilitation of localization of extensional strain by the inherited lithospheric heterogeneity. For example, the width of the northern and southern ends of the rift is identical (~50 km); the border faults in these parts of the rift were developed by reactivation of preexisting Precambrian structures (Figure 3). In contrast, the Central Section appears to be the widest (~75 km) part of the rift, and this is where inherited lithospheric heterogeneity did not favor strong extensional strain localization. For this, we conclude that the presence of inherited lithospheric heterogeneity has been critical in facilitating the segmentation of the Malawi rift during its opening, responding to a general E-W but southward diminishing extension.

6. Conclusions

Our results obtained from the analysis of SRTM DEM highlight the importance of inherited lithospheric heterogeneity in facilitating the segmentation of largely amagmatic continental rifts as exemplified by the portion of the Western Branch of the EARS represented by the Cenozoic Malawi Rift. Pre-existing structures of various Paleoproterozoic to Neoproterozoic terrains facilitated first-order segmentation of the rift into: (1) A Northern Section with preexisting Precambrian structures favoring extensional strain localization within border faults that exploited the inherited lithospheric heterogeneity. (2) A Central Section where

the preexisting Precambrian structures did not favor strong extensional strain localization leading to the development of the rift as a shallow and wider graben with poorly developed border faults. (3) A Southern Section where the preexisting structures allowed for shallow-level lithospheric extensional strain localization producing a rift with no sedimentation-related subsidence and a rift floor that is underlain by Precambrian rocks. The presence of ENE trending grabens of Paleozoic-Mesozoic age presented shallow inherited lithospheric heterogeneity that facilitated second-order segmentation of the Malawi Rift as a conjugate convergent overlapping pattern. This geometry is depicted by the presence of half-grabens/asymmetrical grabens of alternating polarity bounded by four ~150 km long, overlapping and alternating border faults starting with an east dipping northern one. The overlap zones occurring at the transition between rift segments have length to width ratios close to one and these overlap zones host flip-over full-graben. The inherited lithospheric heterogeneity played the major role in the facilitation of segmentation of the Malawi Rift during its opening in response to extension that decreases from north to south.

Acknowledgments

SRTM DEM data used in this study are available from the Jet Propulsion Laboratory of the National Aeronautics and Space Administration. The aeromagnetic data can be obtained from the Geological Survey Department, Malawi. This project is supported by the National Science Foundation – Continental Dynamics grant no. EAR-1255233 and Office of International and Integrative Activities grant no. IIA-1358150. H.S. Al-Salmi was supported by an ExxonMobil scholarship. Emmanuel Njinju drafted the magnetic images. Three anonymous reviewers and Associate Editor Glen Mattioli provided useful comments. This is the Oklahoma State University Boone Pickens School of Geology contribution number 2015-31.

References

Aanyu, K., and D. Koehn (2011), Influence of pre-existing fabrics on fault kinematics and rift geometry of interacting segments: Analogue models based on the Albertine Rift (Uganda), Western Branch-East African Rift System, *J. Afr. Earth Sci.*, *59*(2), 168–184.

Betzler, C., and U. Ring (1995), Sedimentology of the Malawi Rift: Facies and stratigraphy of the Chiwondo Beds, northern Malawi, *J. Hum. Evol.*, *28*(1), 23–35.

Biggs, J., E. Nissen, T. Craig, J. Jackson, and D. Robinson (2010), Breaking up the hanging wall of a rift-border fault: The 2009 Karonga earthquakes, Malawi, *Geophys. Res. Lett.*, *37*, L11305, doi:10.1029/2010GL043179.

Bingen, B., J. Jacobs, G. Viola, I. Henderson, Ø. Skår, R. Boyd, R. Thomas, A. Solli, R. Key, and E. Daudi (2009), Geochronology of the Precambrian crust in the Mozambique belt in NE Mozambique, and implications for Gondwana assembly, *Precambrian Res.*, *170*(3), 231–255.

Calais, E., C. Ebinger, C. Hartnady, and J. Nocquet (2006), Kinematics of the East African Rift from GPS and earthquake slip vector data, *Geol. Soc. London Spec. Publ.*, *259*, 9–22.

Castaing, C. (1991), Post-Pan-African tectonic evolution of South Malawi in relation to the Karroo and recent East African rift systems, *Tectonophysics*, *191*(1), 55–73.

Chorowicz, J. (1989), Transfer and transform fault zones in continental rifts: Examples in the Afro-Arabian Rift System Implications of crust breaking, *J. Afr. Earth Sci.*, *8*(2–4), 203–214.

Chorowicz, J. (2005), The East African rift system, *J. Afr. Earth Sci.*, *43*(1), 379–410.

Chorowicz, J., and C. Sorlien (1992), Oblique extensional tectonics in the Malawi Rift, Africa, *Geol. Soc. Am. Bull.*, *104*(8), 1015–1023.

Contreras, J., M. H. Anders, and C. H. Scholz (2000), Growth of a normal fault system: Observations from the Lake Malawi basin of the east African rift, *J. Struct. Geol.*, *22*(2), 159–168.

Corti, G., J. van Wijk, S. Cloetingh, and C. K. Morley (2007), Tectonic inheritance and continental rift architecture: Numerical and analogue models of the East African Rift system, *Tectonics*, *26*, TC6006, doi:10.1029/2006TC002086.

Ebinger, C., A. Deino, R. Drake, and A. Tesha (1989), Chronology of volcanism and rift basin propagation: Rungwe Volcanic Province, East Africa, *J. Geophys. Res.*, *94*(B11), 15,785–15,803, doi:10.1029/JB094iB11p15785.

Ebinger, C., A. Deino, A. Tesha, T. Becker, and U. Ring (1993), Tectonic controls on rift basin morphology: Evolution of the Northern Malawi (Nyasa) Rift, *J. Geophys. Res.*, *98*(B10), 17,821–17,836, doi:10.1029/93JB01392.

Ebinger, C. J., M. J. Crow, B. R. Rosendahl, D. A. Livingstone, and J. LeFournier (1984), Structural evolution of Lake Malawi, Africa, *Nature*, *308*(5960), 627–629.

Ebinger, C. J., B. Rosendahl, and D. Reynolds (1987), Tectonic model of the Malaŵi rift, Africa, *Tectonophysics*, *141*(1), 215–235.

Flannery, J., and B. Rosendahl (1990), The seismic stratigraphy of Lake Malawi, Africa: Implications for interpreting geological processes in lacustrine rifts, *J. Afr. Earth Sci.*, *10*(3), 519–548.

Fritz, H., M. Abdelsalam, K. Ali, B. Bingen, A. Collins, A. Fowler, W. Ghebreab, C. Hauzenberger, P. Johnson, and T. Kusky (2013), Orogen styles in the East African Orogen: A review of the Neoproterozoic to Cambrian tectonic evolution, *J. Afr. Earth Sci.*, *86*, 65–106.

Hanson, R. E., T. J. Wilson, and H. Munyanyiwa (1994), Geologic evolution of the Neoproterozoic Zambezi orogenic belt in Zambia, *J. Afr. Earth Sci.*, *18*(2), 135–150.

Hargrove, U. S., R. E. Hanson, M. W. Martin, T. G. Blenkinsop, S. A. Bowring, N. Walker, and H. Munyanyiwa (2003), Tectonic evolution of the Zambezi orogenic belt: Geochronological, structural, and petrological constraints from northern Zimbabwe, *Precambrian Res.*, *123*(2), 159–186.

Jackson, J., and T. Blenkinsop (1997), The Bilila-Mtakataka fault in Malaŵi: An active, 100-km long, normal fault segment in thick seismogenic crust, *Tectonics*, *16*(1), 137–150, doi:10.1029/96TC02494.

Katumwehe, A., M. G. Abdelsalam, and E. A. Atekwana (2015), The role of pre-existing Precambrian structures in rift evolution: The Albertine and Rhino Grabens, Uganda, *Tectonophysics*, *646*, 117–129, doi:10.1016/j.tecto.2015.01.022.

Leseane, K., E. A. Atekwana, K. L. Mickus, M. G. Abdelsalam, E. M. Shemang, and E. A. Atekwana (2015), Thermal perturbations beneath the incipient Okavango Rift Zone, northwest Botswana, *J. Geophys. Res. Solid Earth*, *120*, 1210–1228, doi:10.1002/2014JB011029.

McClay, K. R., and M. J. White (1995), Analogue modelling of orthogonal and oblique rifting, *Mar. Pet. Geol.*, *12*(2), 137–151.

McClay, K. R., T. Dooley, P. Whitehouse, and M. Mills (2002), 4-D evolution of rift systems: Insights from scaled physical models, *AAPG Bull.*, *86*(6), 935–960.

Meert, J. G. (2003), A synopsis of events related to the assembly of eastern Gondwana, *Tectonophysics*, *362*(1), 1–40.

Morley, C., R. Nelson, T. Patton, and S. Munn (1990), Transfer zones in the East African rift system and their relevance to hydrocarbon exploration in rifts (1), *AAPG Bull.*, *74*(8), 1234–1253.

Ring, U., and C. Betzler (1995), Geology of the Malawi Rift: Kinematic and tectonosedimentary background to the Chiwondo Beds, northern Malawi, *J. Hum. Evol.*, *28*(1), 7–21.

Ring, U., C. Betzler, and D. Delvaux (1992), Normal vs. strike-slip faulting during rift development in East Africa: The Malawi rift, *Geology*, *20*(11), 1015–1018.

Ring, U., A. Kroner, B. Buchwaldt, T. Toulkeridis, and P. W. Layer (2002), Shear zone patterns and ecologite-facies metamorphism in the Mozambique belt of northern Malawi, east-central Africa: Implications for the assembly of Gondwana, *Gondwana Res.*, *116*, 19–56.

Rosendahl, B. R., E. Kilembe, and K. Kaczmarick (1992), Comparison of the Tanganyika, Malawi, Rukwa and Turkana Rift zones from analyses of seismic reflection data, *Tectonophysics*, *213*(1), 235–256.

Saria, E., E. Calais, D. Stamps, D. Delvaux, and C. Hartnady (2014), Present-day kinematics of the East African Rift, *J. Geophys. Res. Solid Earth*, *119*, 3584–3600, doi:10.1002/2013JB010901.

Specht, T. D., and B. R. Rosendahl (1989), Architecture of the Lake Malawi rift, east Africa, *J. Afr. Earth Sci.*, *8*(2), 355–382.

Stamps, D. S., E. Calais, E. Saria, C. Hartnady, J.-M. Nocquet, C. J. Ebinger, and R. M. Fernandes (2008), A kinematic model for the East African Rift, *Geophys. Res. Lett.*, *35*, L05304, doi:10.1029/2007GL032781.

Van der Beek, P., E. Mbede, P. Andriessen, and D. Delvaux (1998), Denudation history of the Malawi and Rukwa Rift flanks (East African Rift System) from apatite fission track thermochronology, *J. Afr. Earth Sci.*, *26*(3), 363–385.

Van Wijk, J. W. (2005), Role of weak zone orientation in continental lithosphere extension, *Geophys. Res. Lett.*, *32*, L02303, doi:10.1029/2004GL022192.

Versfelt, J., and B. Rosendahl (1989), Relationships between pre-rift structure and rift architecture in Lakes Tanganyika and Malawi, East Africa, *Nature*, *337*, 354–357.